Heterocycles as Supramolecular Handles for Engineering: A Case Study with 7-(Diethylamino)coumarin Derivatives

Geraldyne Castro,[a] Margarita Romero-Ávila,[a] Norberto Farfán,[a]* Rafael Arcos-Ramos,[c]* and Mauricio Maldonado-Domínguez.[a]*

[a] Facultad de Química, Departamento de Química Orgánica, Universidad Nacional Autónoma de México, Ciudad de México, México.

[b] Departamento de Química de Radiaciones y Radioquímica, Instituto de Ciencias Nucleares, Universidad Nacional Autónoma de México, Ciudad de México, México.

*email: maldonado86@quimica.unam.mx

Abstract

In this study, we present the synthesis and detailed solid-state structural characterization of a Schiff-base-bridged derivative of 7-(Diethylamino)coumarin (DAC) to carry out a comparative crystallographic analysis, within the broader context of a curated dataset of 50 DAC-containing molecules, retrieved from the literature, and their corresponding crystal packing. We uncover that the DAC moiety leverages its pronounced local dipole moment and inherently planar configuration to facilitate different modes of π-stacking interaction. These are strongly directed by C-H···O interactions between the coumarin carbonyl group with the ethyl-residue or the 3-substituent of adjacent molecules. In solution, the presence of a 7-diethylamino group is shown to enhance solubility through its conformational flexibility, while in the crystalline matrix it primarily acts as a structural spacer that favors π-stacking interactions. Our findings present a comprehensive analysis of the preferential arrangements of the DAC fragment in various (supra)molecular scenarios, including cases where its influence is overridden. We thus present the entire 7-(Diethylamino)coumarin block as (a) mobile but mostly planar, (b) prone to antiparallel aggregation, and (c) 90% likely to pack via π-stacking supported by hydrogen-bonding interactions, enriching the palette of supramolecular motifs for the programmed assembly of molecular solids.

Introduction

Molecular materials are continuous phases whose smallest components are molecules. These materials, frequently encountered as glassy or crystalline solids, are held together mainly by non-covalent intermolecular interactions, weaker and less directional than the covalent and ionic bonds present in continuous materials such as diamond, glass, and table salt. Constructing a molecular material requires encoding in molecular structures the necessary information to assemble a macroscopic phase, ideally with precise characteristics and predictable behavior. This *bottom-up* approach to the design of molecular materials can strongly accelerate the advance of urgent technologies like cleaner light sources,[1] ultradense storage of digital data,[2,3] efficient sunlight harvesting,[4] and the miniaturization of electronic devices.[5]

Such encoding of macroscopic properties into microscopic and discrete molecular structures is one of the challenges in developing molecular materials.[6–9] There are functional groups prone to dictate aggregation, like carboxylic acids which form H-bonded dimers in solution,[10] and nucleobases, which readily associate via complementary H-bonding interactions to form DNA (**Figure 1**).[11,12]

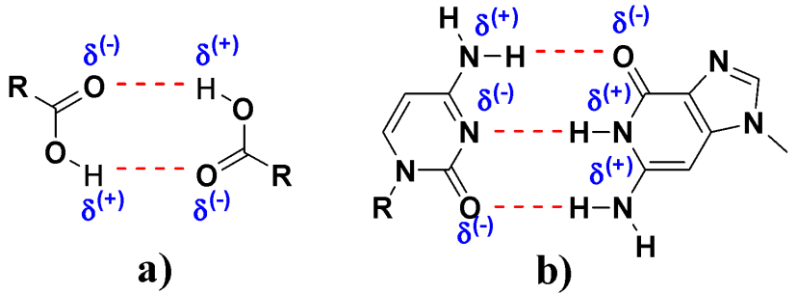

Figure 1. Hydrogen bonding motifs in **a)** carboxylic acids and **b)** Watson-Crick pairing of nucleobases in DNA and RNA.

As these examples show, functional groups that can engage in H-bonding tend to tailor aggregation due to the strength and directionality of hydrogen bonds, which make them effective handles for supramolecular assembly.[13] In addition to H-bonds, halogen bonds,[14] and π-stacking between aromatic rings,[15,16] are recognized interactions in the supramolecular

palette for the construction of molecular materials. Therefore, an ideal target molecule must display not only a desired and quantifiable electronic property or response, like luminescence or charge-carrier conductivity, but it must also possess a molecular structure that directs the supramolecular assemblage of the material from the bottom-up, to display the desired property.

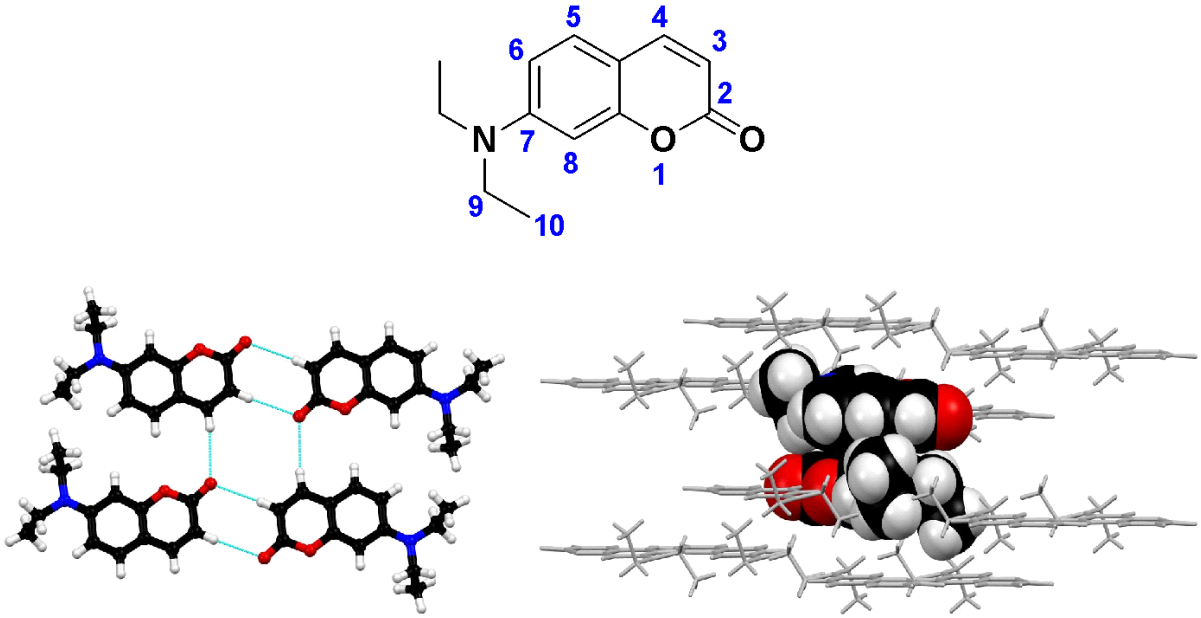

Figure 2. Molecular structure of 7-diethylaminocoumarin, DAC, a functionalized heterocycle that often forms molecular crystals, connected through C-H···O, with extensive π-stacking.

In the context of programmable molecular aggregation, we investigate the viability of heterocyclic fragments as *structure-directing groups*, SDGs. Heterocycles engage in π-stacking like their carbocyclic counterparts, and the heteroatoms in their structure imbue them with distinct polarities and H-bonding capabilities. From the vast ecosystem of heterocyclic rings, we currently investigate coumarins which, in our experience, tend to form crystalline solids effortlessly.[17–19] Derivatives of 7-(Diethylamino)coumarin (DAC, **Figure 2**) stands out in this respect, because (*a*) they are prone to spontaneous crystallization, (*b*) their crystals often feature extensive stacking of the coumarin heterocycle, and (*c*) DAC-derivatives tend to be reasonably soluble in common organic solvents. If the DAC fragment exhibits well-defined aggregation modes irrespective of its functionalization, it can be employed as an SDG to tailor

the packing of target molecular blocks during the design and construction of molecular materials.

In this study, we investigate the preferred aggregation modes of 7-(Diethylamino)coumarin and all of its crystalline derivatives reported to date in the Crystallography Open Database,[20–23] as supramolecular synthons for the programmed assembly of molecular solids and clusters. Our approach begins by comparing all molecular crystals featuring the DAC group and whose crystal structure has been solved and deposited on public databases, to assert whether its orientation and non-covalent interactions in molecular solids are predictable and useful as structure-directing groups, SDGs. Then, we present the synthesis, characterization, and crystal structure of a novel Schiff-base-bridged DAC derivative, and we compare its solid-state structure with the full set of crystalline DAC-derivatives retrieved from the literature. Finally, we computed frontier molecular orbital energies of all the studied compounds, using Density Functional Theory, charting this way the structural and energetic landscape of the DAC group in its known molecular contexts. With this study, we seek to expand the understanding of noncovalent interactions in polar heterocycles, striving to enrich the palette of molecular handles to tailor the bottom-up design of materials with desirable properties.

MATERIALS AND METHODS

Experimental Section

All reagents used were obtained from commercial suppliers and used without further purification. Solvents were dried using standard methods or distilled prior to use. Reactions were monitored by TLC on precoated silica gel plates (Aldrich Silica gel on TLC plates with 254 nm fluorescent indicator) and revealed by exposure to a UV lamp. ^{1}H and ^{13}C NMR spectra were recorded using a Bruker 400 MHz spectrometer; chemical shifts (δ, ppm) are reported relative to $CDCl_3$. High-resolution mass spectra were acquired with an Agilent Technologies ESI TOF spectrometer.

Synthesis of 7-(diethylamino)coumarin-3-carbaldehyde, compound 2.

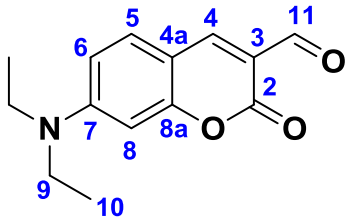

Compound **2** was synthesized from 4-(diethylamino)salicylaldehyde in two steps according to a literature procedure,[24,25] to give an orange crystalline solid. Yield: 79%. Rf = 0.2 (hexane/ethyl acetate, 8:2). Melting point 163–165 °C. ^{1}H-NMR (400 MHz, $CDCl_3$, δ, ppm): 10.10 (s, 1H, H-11), 8.23 (s, 1H, H-4), 7.40 (d, J = 9.0 Hz, 1H, H-5), 6.62 (dd, J = 9.0, 2.5 Hz, 1H, H-6), 6.47 (d, J = 2.5 Hz, 1H, H-8), 3.46 (q, J = 7.2 Hz, 4H, H-9), 1.24 (t, J = 7.2 Hz, 6H, H-10). ^{13}C-NMR (75 MHz, $CDCl_3$, δ, ppm): 188.0 (C-11), 162.0 (C-2), 159.0 (C-8a), 153.6 (C-7), 145.5 (C-4), 132.6 (C-5), 114.4 (C-3), 110.3 (C-6), 108.3 (C-4a), 97.2 (C-8), 45.4 (C-9), 12.6 (C-10).

Synthesis of (*E*)-3-(((4*H*-1,2,4-triazol-4-yl)imino)methyl)-7-(diethylamino)-2*H*-chromen-2-one:

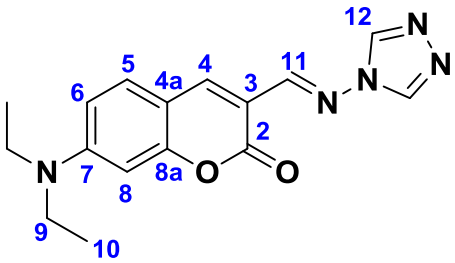

In a round bottom flask equipped with a Dean-Stark distillation trap, 4-amino-4*H*-1,2,4-triazole (0.017 g, 0.2 mmol) and **7-(Diethylamino)coumarin-3-carbaldehyde** (0.05 g, 0.2 mmol) were suspended in 5 mL of a 2:1 mixture of EtOH and toluene. The mixture was stirred at reflux temperature for 150 h, frequently draining the Dean-Stark trap and adding more solvent mixture accordingly (**Scheme 1**). The product was formed as an orange precipitate. The solution was cooled in an ice bath, the solid was filtered and washed with cold toluene. The crude product was purified by chromatography on silica gel, starting with CH_2Cl_2 100%, followed by a linear gradient of CH_2Cl_2:Acetone up to an 8:2 v/v ratio, to give the product as a bright orange solid that grows crystals from CH_2Cl_2 (0.16 mmol, 50 mg, 80 %). Rf = 0.15 (CH_2Cl_2: Acetone 9:1). Melting point (*from* CH_2Cl_2): 238–240 °C. FTIR (ATR, ν, cm^{-1}): 3105, 3080, 2968, 2950,

2930, 1701, 1603, 1570, 1516, 1502, 1478, 1424, 1351, 1255, 1188, 1180, 1127. ^{1}H-NMR (400 MHz, $CDCl_3$, δ, ppm): 8.75 (s, 1H, H-11), 8.57 (s, 2H, H-12), 8.40 (s, 1H, H-4), 7.40 (d, J = 9.0 Hz, 1H, H-5), 6.65 (dd, J = 9.0, 2.5 Hz, 1H, H-6), 6.49 (d, J = 2.5 Hz, 1H, H-8), 3.46 (q, J = 7.2 Hz, 4H, H-9), 1.24 (t, J = 7.2 Hz, 6H, H-10). ^{13}C-NMR (75 MHz, $CDCl_3$, δ, ppm): 161.4 (C-2), 158.1 (C-8a), 153.0 (C-7), 151.8 (C-11), 142.2 (C-4), 138.3 (C-12), 131.5 (C-5), 110.3 (C-6), 110.1 (C-3), 108.5 (C-4a), 97.3 (C-8), 45.3 (C-9), 12.6 (C-10). HRMS (ESI-TOF): calcd. for $C_{16}H_{17}N_5O_2$+H 312.1460, found $[C_{16}H_{17}N_5O_2+H]^+$ 312.1455. Error: 2.242540 ppm.

Database search, retrieval, and curation of experimental XRD data

A search on the Crystallography Open Database (05/02/2024),[20–23] using 7-(Diethylamino)coumarin as parent fragment, produced a total of 82 crystal structures. Solvates, cocrystals, and molecules not containing the DAC fragment were excluded from our analysis. We found 50 distinct molecules and 52 distinct crystals structures (two of them presenting polymorphism) fulfilling these criteria, and the corresponding structural data was retrieved as CIF files. Database IDs and structural parameters of all the retrieved cells are condensed in **Table S2**.

Single X-Ray Diffraction Experiments

A suitable single crystal of compound **11** was mounted on a glass fiber. Crystallographic data were collected with an Oxford Diffraction Gemini Atlas diffractometer with a CCD area detector; the radiation using a monochromator of graphite with $\lambda_{MoK\alpha}$ = 0.71073 Å, at 120 K. The double pass method of scanning was used to exclude any noise. The collected frames were integrated by using an orientation matrix determined from the narrow frame scans. CrysAlisPro and CrysAlisRED software package[26] were used for data collection and integration. Analysis of the integrated data did not reveal any decay. Collected data were corrected for absorption effects by a numerical absorption correction[27] using a multifaceted crystal model based on expressions upon the Laue symmetry with equivalent reflections. The structure solution and refinement were carried out with the OLEX2 analysis program.[28] Mercury[29] was used to prepare artwork representations material for publication. Full-matrix least-squares refinement was carried out by minimizing $(Fo^2 - Fc^2)^2$. All non-hydrogen atoms were refined

anisotropically. Hydrogen atoms attached to carbon atoms were placed in geometrically idealized positions and refined as riding on their parent atoms, with C—H = 0.95 – 0.99 Å with Uiso (H) = 1.2Ueq(C) for aromatic and methylene groups, and Uiso (H) = 1.5 Ueq(C) for methyl groups. Crystallographic data have been deposited at the Cambridge Crystallographic Data Center as supplementary material CCDC: 2338583. Copies of the data can be obtained free of charge on application to CCDC, 12 Union Road, Cambridge CB2 1EZ, UK. e-mail: deposit@ccdc.cam.ac.uk. The structural cell parameters of compound **11** are condensed in **Table S1**.

Density Functional Theory Calculations

We optimized all molecular geometries using the MN15 density functional[30] with the def2TZVP basis set.[31] Convergence thresholds for this procedure were: 10^{-8} Ha for energy gradients, 1.8×10^{-4} Ha/Å for maximum force, and 4.5×10^{-4} Å for maximum atomic displacement. Vibrational frequencies were calculated with the same scheme, using the harmonic approximation, observing only real frequencies for all minima and a single imaginary frequency for transition states. We approximated the polarity of a molecular crystal as a continuum of dielectric constant ε = 3.5, which is the average of the value range observed experimentally for polar molecules, from ε = 2 to ε = 5.[32,33] The Conductor-like Polarizable Continuum Model, CPCM.[31,34] was employed for this task, with ε = 3.5. Final electronic potential energies were calculated with the def2TZVP basis set, to minimize truncation errors due to the use of a finite basis set. For brevity, the DFT method just described, MN15(CPCM)/def2TZVP, will be referred to simply as *the DFT protocol* throughout this work. Frontier molecular orbital energies were calculated using time-dependent DFT with the DFT protocol, allowing 20 states in the configuration interaction singles (CIS) procedure.[35–37] Results from calculations are condensed in the Supporting Information file, in **Table S4**.

RESULTS AND DISCUSSION

Synthesis of a Schiff-base-bridged DAC-derivative and analysis of its crystal structure

This study investigates the potential of the DAC moiety as a structure-directing group, capable of spontaneous self-assembly into predictable supramolecular arrangements. As part of our tests, we currently explore the incorporation of nitrogenated rings into the DAC-core. In particular, 4-amino-1,2,4-triazole **51** crystallizes via hydrogen bonding interactions [N-H···N, chains] in its pure form (**Figure 3**).

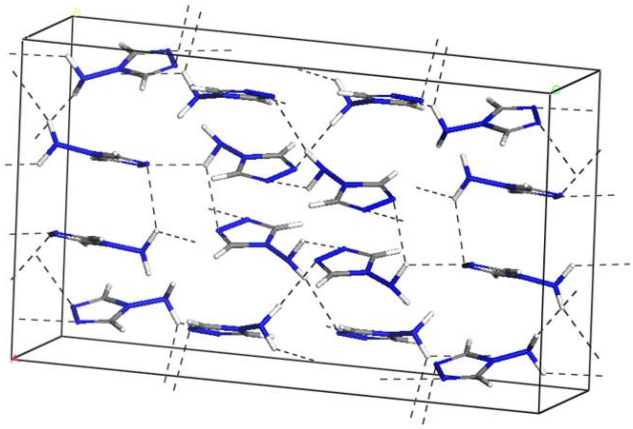

Figure 3. Three-dimensional array of H-bonded molecular units of 4-amino-1,2,4-triazole, **51**, in the crystal phase.

The presence of the amino group (-NH_2) in **51** suggests an imino-bond (Schiff base) as a suitable π-bridge for the formation of a new π-extended DAC derivative (**Scheme 1)**. Imine linkers lack the H-bond donating capability of the parent amino-triazole due to the replacement of the hydrogens with a C=N double bond, suppressing classical H-bonding and producing alternative packing arrangements in the solid-state that tend to be governed by dipolar interactions and planar π-stacking. A detailed spectroscopic characterization of **11** is presented as electronic supporting information.

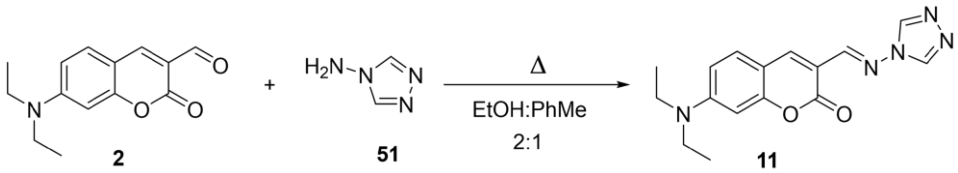

Scheme 1. Synthesis of **Compound 11**.

Analysis of molecular crystals containing the DAC moiety

The full set of 50 DAC-substituted coumarins considered in this study, labeled **1-50**, is presented in **Figure 4**. The crystal structure for compound **11** is reported in this work. Crystals structures for **1-10** and **12-50** were retrieved from the Crystallography Open Database. All crystals were inspected for the presence or absence of planar π-stacking, defined as interplanar distance, d_{stack} less or equal to 4.5 Å, between existing π-systems. We found that 47 out of 52 (90%) examples present various forms of planar π-stacking.

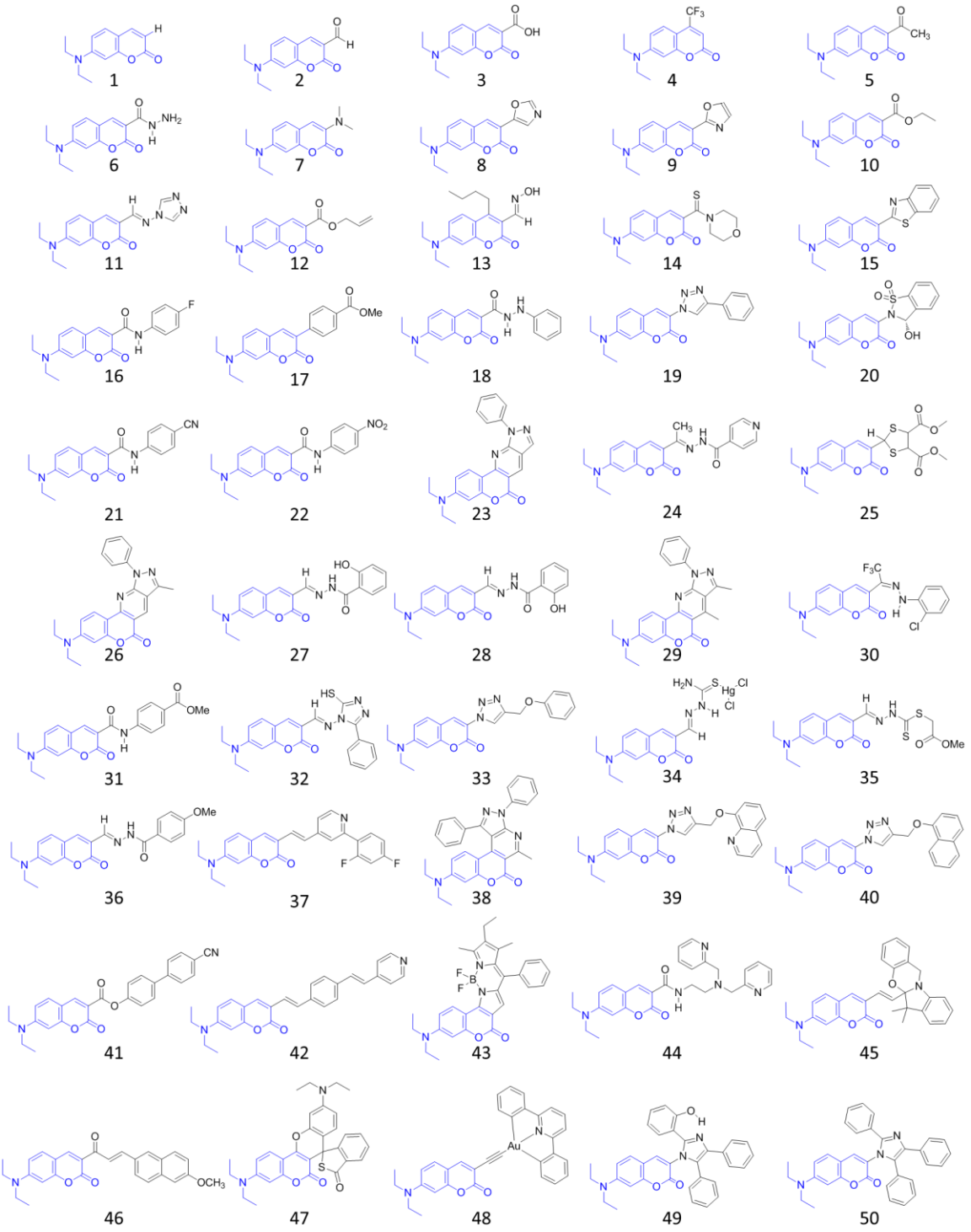

Figure 4. Molecular structure of 7-(Diethylamino)coumarin (DAC-H, compound **1**), and all DAC-containing derivatives analyzed in this work and retrieved from the Crystallographic Open Database.

In general, the coumarin core is intrinsically π-delocalized due to its conjugated nature; thus, depending on its substitution pattern, different modes of electron delocalization may translate, in principle, into distinct aggregation modes. In this context, the DAC-H parent compound **1** displays a full anti-parallel π-stacking in both available polymorphs, derived from cyclic C-H···O interactions between adjacent coumarins and supported by ethyl residues [**Figure 2**].[17] The DAC-core utilizes the carbonyl group as a supramolecular synthon, exhibiting synergistic interactions with diverse substituents at positions C-4 and C-3 of the coumarin heterocycle, facilitating an anti-parallel coumarin alignment and promoting various forms of planar π-stacking.

The incorporation of relatively simple substituents (**2**, **3**, **4**, **5**, **6**, **7**, **8**, **10**, **12**) does not alter the ability of the carbonyl group within the DAC-core to direct self-assembly through hydrogen bonding interactions [C-H···O, C=O···C=O] (coumarin - coumarin, coumarin - ethyl); these strong, primary interactions cooperate with weaker complementary interactions [C-H···O, C-H···N, N-H···O] mainly established by the substituents (coumarin-substituent, ethyl-substituent, substituent-substituent) [**Figure 5**].

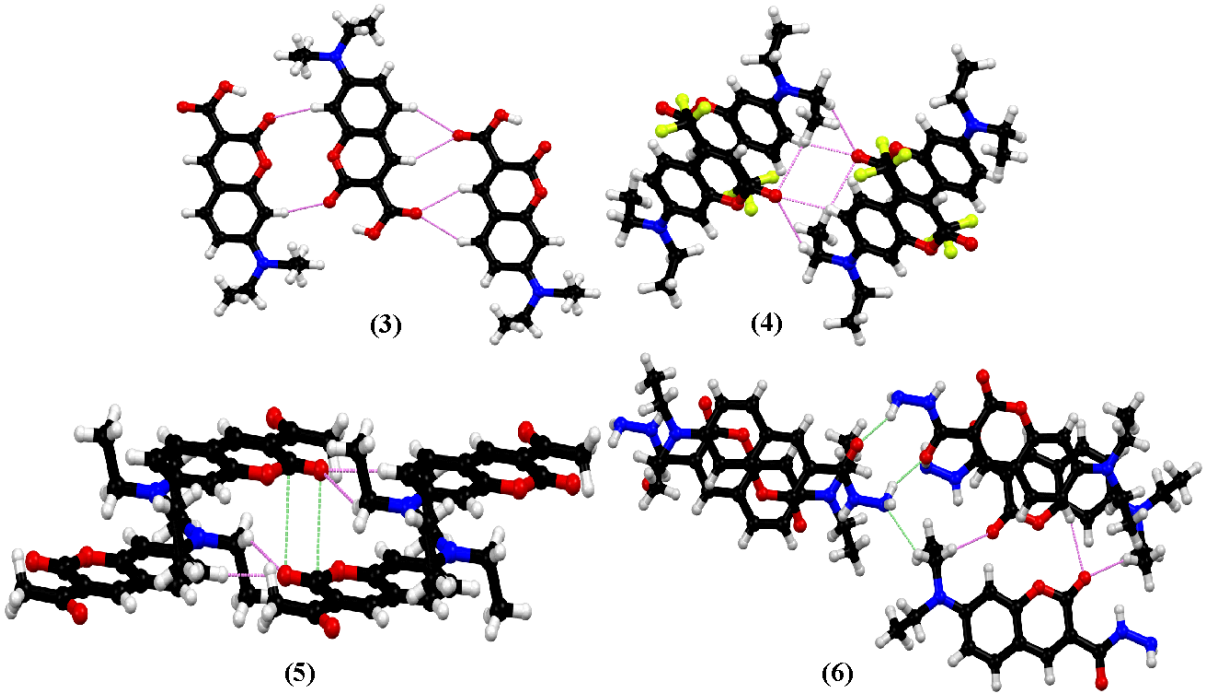

Figure 5. Selected examples illustrate how the carbonyl group in position C2 of the coumarin heterocycle acts as a versatile handle in different supramolecular assemblies, demonstrating a cooperative effect with various substituents.

Introducing more structurally complex substituents, like rings or fused cycles, does not hinder the carbonyl group's ability to direct self-assembly through hydrogen bonding or dipolar interactions [C-H···O, C-H···N, C=O···C=O]. Coumarin molecules are generally aligned in an anti-parallel fashion enabling diverse π-stacking modes governed by the substituent structure and interaction capabilities, such as planarity and stackable surface [**Figure 6**].

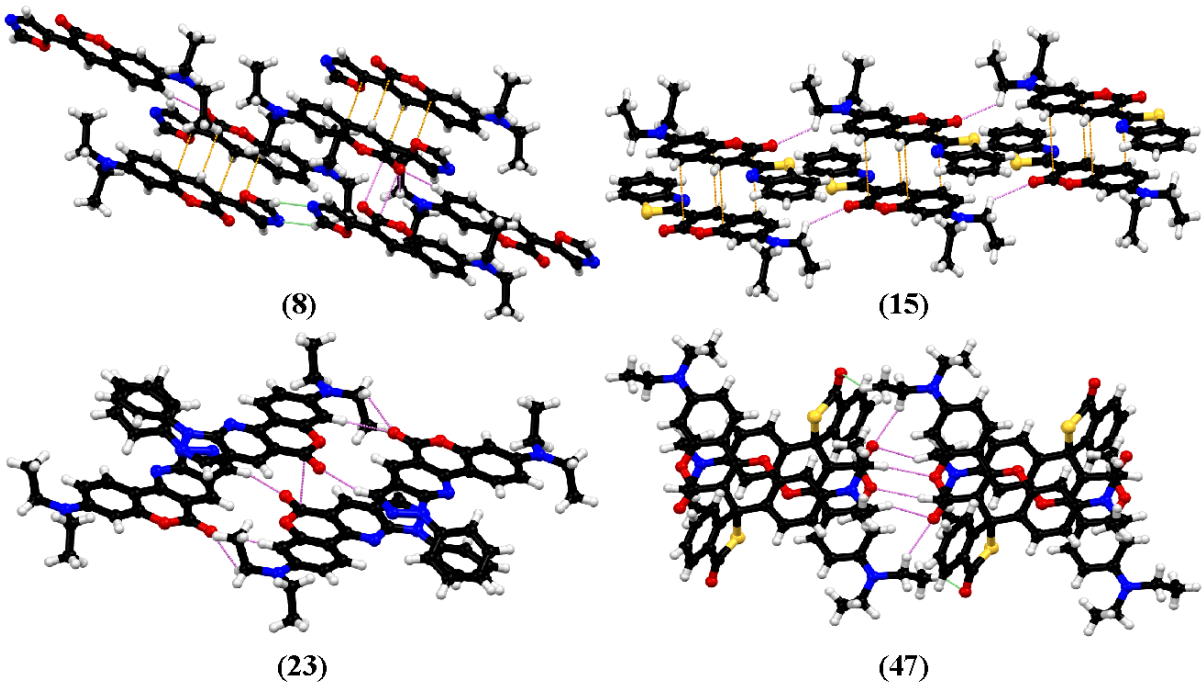

Figure 6. Selected examples to show how the carbonyl group acts as a building block within supramolecular assemblies, showcasing its cooperative effect with complex substituents like rings or fused cycles.

In certain instances, the structural features of the substituent (exemplified by compounds **32** and **43**) such as size, shape, and interaction capabilities, influence or override the formation of the typical one-dimensional arrangements of parallel or anti-parallel coumarin alignments. Such exceptional cases are self-assembled through interactions driven by the substituent, favoring the π-stacking between these motifs. This effect is further amplified in DAC-derivatives **48** and **50**, where interactions within the core structure act as spacers, allowing the substituent to form various two-dimensional π-stacked assemblies [**Figure 7**].

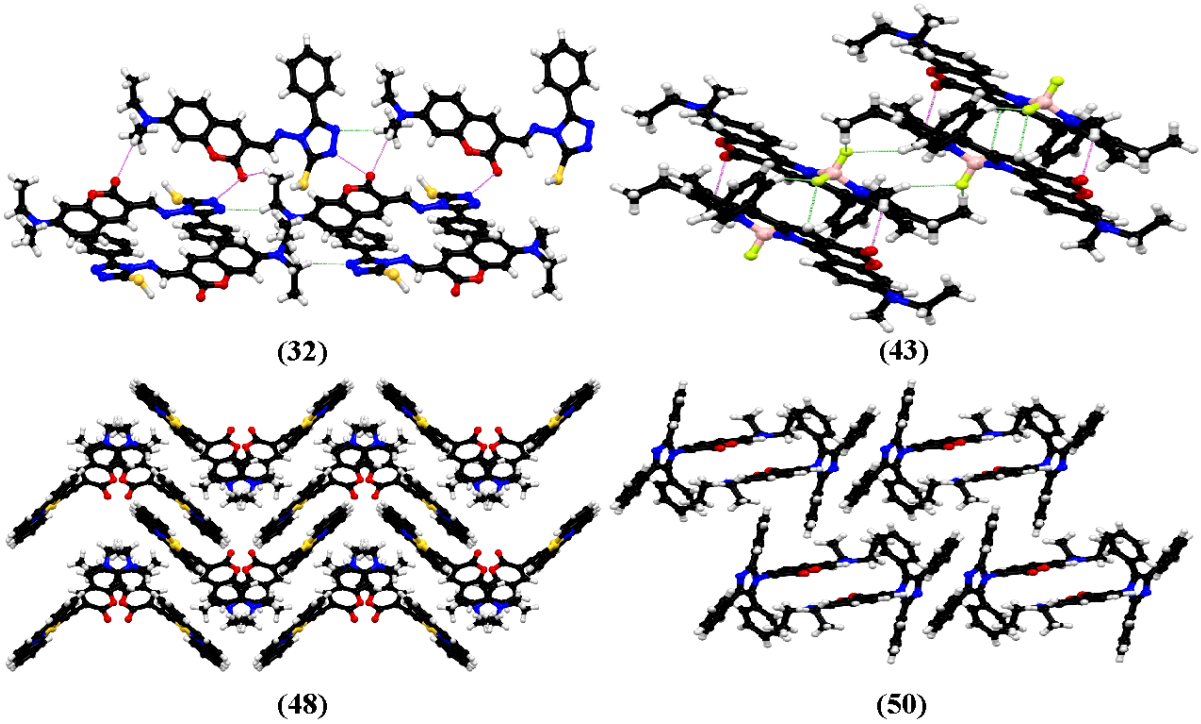

Figure 7. Selected examples showing how the carbonyl group acts as the main structure-directing element when coumarin π-stacking is overridden.

Compound **11** was obtained as a crystalline orange solid, soluble in polar solvents, protic and aprotic, like AcOEt and EtOH. Suitable crystals for single X-Ray diffraction were obtained for **11 (from DCM)**, relevant crystallographic data is summarized in Tables S2 and S3 (see ESI). The crystal structure was solved in the monoclinic space group P 2_1/c with one molecule per asymmetric unit (Z = 4, Z' = 1) [**Figure 8A**]. A detailed analysis of the crystal packing demonstrated that the carbonyl group interacts with the triazole ring by cyclic hydrogen bonding interactions [C-H···O, R^1_2 (7), *ca.* 2.54 Å], leading to the anti-parallel alignment of molecules [**Figure 8B**], which produce a one-dimensional layer through cyclic hydrogen-bonding between the ethyl residues and the triazole ring [C-H···O, R^2_2 (8), *ca.* 2.67 Å] [**Figure 8C**]**.** These layers interact through complementary hydrogen bonding interactions between coumarin cores [C-H···O, *ca.* 2.55 Å], resulting in a multilayered self-assembled π-stacked structure. This finding emphasizes the combined influence of a functional group within a core structure (carbonyl group and ethyl residue) and a substituent (triazole) on the self-assembly process.

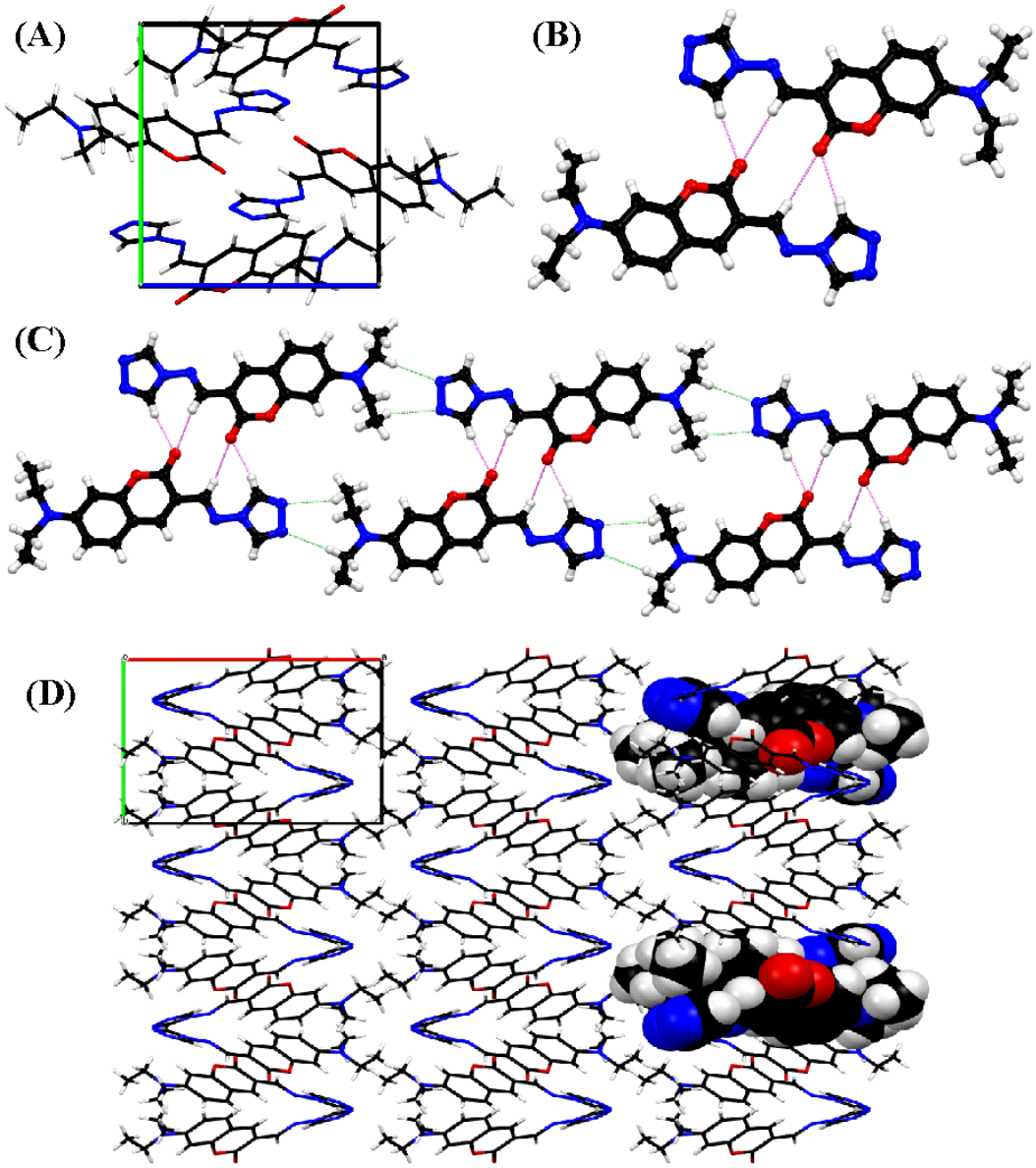

Figure 8. Crystal structure analysis of **11:** (A) unit cell, relevant hydrogen-bonding interactions between the (B) coumarin-substituent and (C) ethyl-substituent. (D) Multilayered π-stacked arrangement.

Molecular and electronic structure of the DAC-H parent block

The DAC-H parent compound **1** possesses a strong ground-state permanent dipole, μ_{DAC} = 6.97 D (**Figure 7A**), calculated with the DFT protocol described in *Materials and Methods*. For comparison, the dipole moments of water and dimethylsulfoxide, two archetypal polar molecules, estimated with the same method are μ_{H2O} = 1.85 D and μ_{DMSO} = 4.06 D, respectively.

Therefore, the frequent appearance of antiparallel π-stacking in crystalline DAC-derivatives (**Figure 9B**), is a combination of electrostatic and geometric features. The electrostatic potential map on the molecular surface of **1** displays a complex pattern of locally positive and negative regions (**Figure 9A**), which are self-complementary as evinced by the propensity of the DAC fragment to form stacked supramolecular dimers. As shown in **Figure S6**, the molecular dipole moments μ calculated with the DFT protocol for a set of reference molecules lie within 10% of their experimental values, supporting our choice DFT protocol.

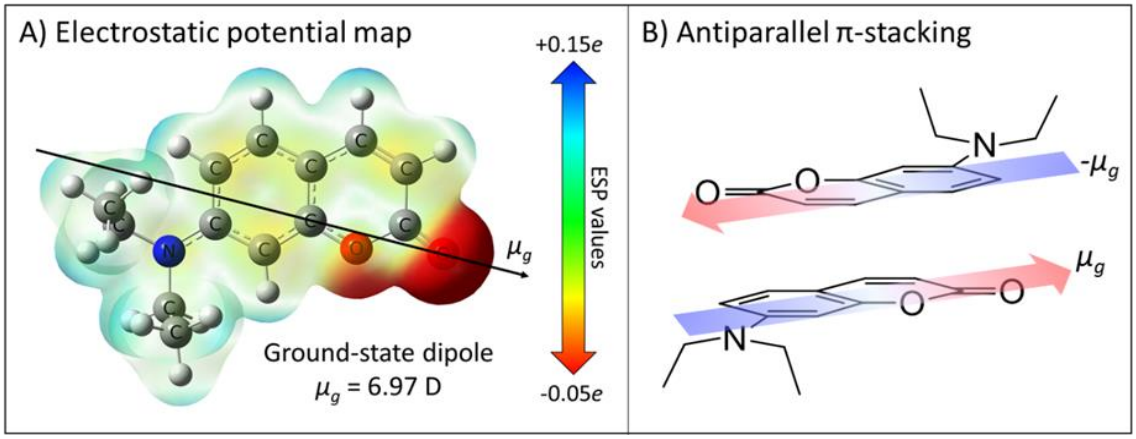

Figure 9. **A.** The strong dipole moment of the 7-diethylaminocoumarin (DAC-H) parent compound **1**, and the electrostatic potential (ESP) map on the surface of its molecular electron density. **B.** The antiparallel π-stacking of DAC fragments, a common motif in DAC-containing molecular crystals, can be seen as a combination of dipole-dipole interaction and planar intermolecular contacts.

The dynamic nature of the pendant 7-diethylamino group in DAC is as important as its electronic properties for the observed trends. Besides contributing to the polarity of this building block through the *push-pull* effect,[18,19] the pendant Et_2N- group contributes entropically to the solubility of a compound incorporating it, following:

$$S_{conf} = -R \sum_i \quad p_i ln(p_i) \qquad (1)$$

Where S_{conf} is the molecular conformational entropy, R is the universal gas constant and p_i is the Boltzmann probability of the ith conformational microstate, calculated as:

$$p_i = \frac{N_i}{N} = -\frac{e^{-Ei/RT}}{\sum_N \quad e^{-E/RT}} \qquad (2)$$

Where N_i is the population of microstate *i*, and *N* is the entire population. Each Et_2N- group that is released from the solid state (where it is conformationally frozen) into the liquid phase, gains torsional degrees of freedom. A static conformational analysis of DAC-H using the selected DFT protocol reveals (**Figure 10**) that its 7-diethylamino group in solution exists as an ensemble of seven conformers in rapid equilibrium. At room temperature, this compact space of rotamers provides a conformational entropy term, $-T\Delta S_{conf}$ = -0.7 kcal mol^{-1}, which contributes to the solubilization by:

$$\frac{K_{Et_2N}}{K_{Solid}} = e^{-(\Delta S/R)} \simeq 3.21 \qquad (3)$$

The result from Equation 3 implies that the sevenfold increase in the total number of conformational microstates from the solid state to the solution phase triples the equilibrium constant towards dissolution, compared to a rigid group with no flexibility. Importantly, the size and shape of the ethyl chains are sufficiently small to allow dense packing in the solid state in all DAC-containing molecular crystals, a potentially useful balance between solubility and unhindered dense stacking.

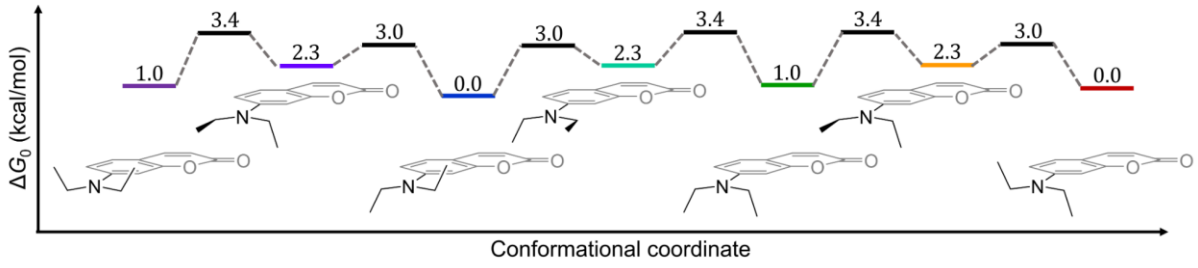

Figure 10. The conformational space of 7-(Diethylamino)coumarin features seven accessible microstates, separated by low free-energy barriers to the torsion of the pendant ethyl chains.

As a final remark to this section, the highest torsional barrier in **Figure 10** has a height of 3.4 kcal/mol which, approximated as a first-order process following Eyring´s transition state theory:

$$k = \frac{k_B T}{h} e^{-(\Delta G^{\neq}/RT)} \qquad (4)$$

corresponds to a rate constant k = 1.0 x 10^{10} s^{-1} and a conversion half-life $t_{1/2}$ = 1.0 x 10^{-10} s^{-1}. In contrast, rotation around the C-N bond connecting the Et_2N- and coumarin-7-yl moieties

costs between 12.3 and 12.7 kcal/mol, with correspondingly longer conversion times (**Figure S7**). Therefore, the Et_2N- group contributes to solubility by means of its conformational entropy, dominated by the flexibility of the pendant ethyl chains.

Frontier molecular orbital energies of DAC-containing molecules

Electron energy levels in continuous materials are delocalized as *bands* and electronic transitions occur mainly near the highest-energy occupied and the lowest-energy unoccupied bands, known as the *valence* and *conduction* bands, respectively. In conductors, these bands overlap, while semiconductor materials display an *energy gap* between the valence and conduction bands. In contrast, discrete molecular materials localize most of their electron density on individual molecules, and their corresponding electron transitions tend to be similarly localized. Such scenario typically involves the *highest occupied* and *lowest unoccupied* molecular orbitals (HOMO and LUMO), apart by a *HOMO-LUMO gap* akin to inorganic semiconductors.[38] Importantly, the energy eigenvalues of the *frontier molecular orbitals*, HOMO and LUMO, are accessible through quantum chemical calculation.

In optoelectronic materials, the luminescent or semiconducting response of a given molecular material tends to correlate with frontier molecular orbital (FMO) energy values, which serve as proxies of the ionization potential (IP) and electron affinities (EA) of the molecule, critical parameters for candidate discrimination and selection of suitable electrode for implementation into electronic devices.[39–41] Frontier molecular orbital energies were calculated using the selected DFT protocol, based on an accurate density functional from the Minnesota family (MN15) a global hybrid functional with excellent performance in scenarios with electron degeneracy, as is the case of organic molecules with extensive π conjugation. Details are provided in the *Materials and Methods* section and the scatter of FMO values for all compounds **1**-**50** are presented in **Figure 11**. All numerical values for FMO energies and optimized molecular geometries are provided in SI.

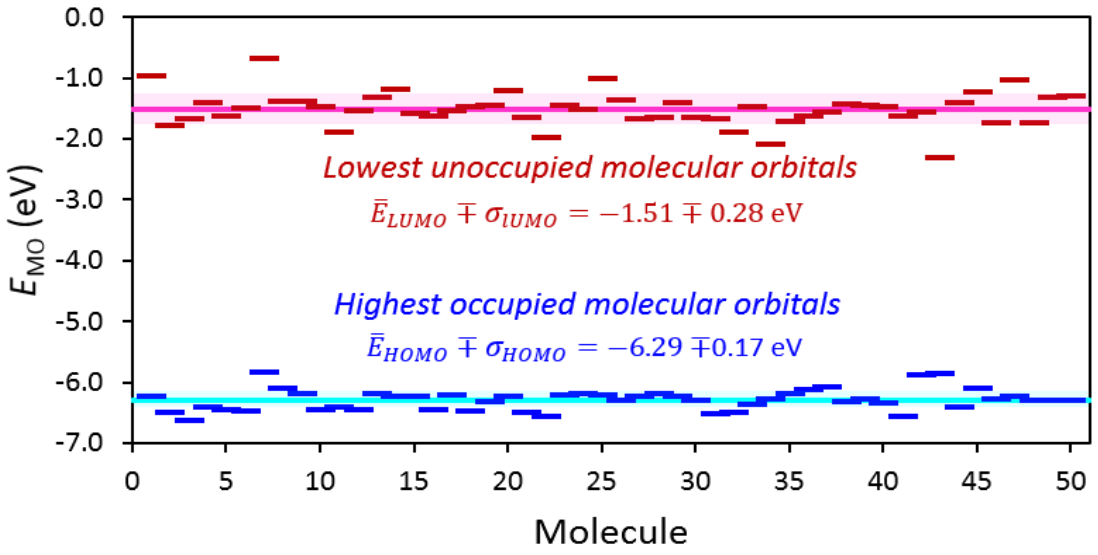

Figure 11. Frontier molecular orbital (FMO) energies of compounds **1-50**, calculated at the MN15(CPCM)/def2TZVP level using density functional theory. Average FMO energies are represented by continuous lines, in colors cyan for E_{HOMO} and magenta for E_{LUMO}. Deviations from the mean are shown as colored areas around each average line, enclosing ±σ, one standard deviation. All energies are expressed in electronvolts.

As shown in **Figure 11**, FMO energies for the existing DAC derivatives are mostly centered around $\bar{E}_{HOMO \pm \sigma HOMO} = -6.29 \pm 0.17$ eV, which is in the range of values (-6.6 to -4.4 eV) reported for *n*-type semiconductors.[42] The average LUMO energy is $\bar{E}_{\mathrm{LUMO} \pm \sigma \mathrm{LUMO}} = -1.51 \pm 0.28$ eV, within the range of values (-1.2 to -3.6 eV) reported for *p*-type semiconductors. This behavior shows that the electronic structure of coumarin derivatives allows not only their use as handles for the design of molecules with programmable aggregation, but also as contributors to the desirable physical properties of the molecular materials built upon it.

Summarizing, we presented a detailed structural and electronic characterization of the 7-(Diethylamino)coumarin heterocyclic moiety, DAC, whose rigidity, planarity, and strong electric dipole allow its use as an unconventional structure-directing functional group. DAC can be readily incorporated as a substituent, leading aggregation by a combination of antiparallel stacking and H-bonding in 90% of the known experimental examples. We synthesized and crystallized a highly nitrogenated DAC-derivative **11**, which followed the general observed trend. Therefore, heterocyclic fragments can be incorporated into the palette

of structure-directing groups available to the crystal engineer if their preferred aggregation is thoroughly characterized, as we did for DAC in this work.

Conclusions

The coumarin heterocycle displays a strong propensity for planar π-stacking, a feature that can be employed to direct the aggregation of molecules into self-assembled molecular materials. In this work, we compared all available molecular crystals, including one new examples recently obtained in our group, containing the 7-(Diethylamino)coumarin (DAC) fragment, which we have consistently observed as a structure-directing group (SDG) dictating the supramolecular arrangement in molecular crystals. We found that 90% of the 52 reported molecular crystal structures containing the DAC fragment display planar π-stacking, imposed by the coumarin planar structure and its strong electric dipole moment. We obtained a new molecular crystal containing the DAC moiety, displaying the same general pattern of aggregation in the crystal phase showcased by DAC-decorated compounds. The 7-diethylamino group is a key component of DAC, contributing to (i) the strong electric dipole present in DAC, and (ii) the solubility of DAC-containing compounds due to its favorable conformational entropy. Electronically, DAC-derivatives can behave as *n*-type and *p*-type semiconductors, and can therefore be versatile building blocks for the design of supramolecular arrangements with precisely tuned electronic structures.

Author Contributions

Geraldyne Castro: investigation, methodology, and writing – original draft. Margarita Romero-Ávila: investigation, methodology. Norberto Farfán: funding acquisition. Rafael Arcos-Ramos: investigation, methodology, formal analysis, data curation, and writing – review and editing. Mauricio Maldonado-Domínguez: conceptualization, software, investigation, data curation, and writing – review and editing, project administration.

Conflicts of interest

There are no conflicts to declare.

Acknowledgments

G. L. C. H. acknowledges CONAHCYT for the granted Ph.D. scholarship (CVU 72652). R. A. R. acknowledges IN-100722 (DGAPA-PAPIIT). M. M. D. acknowledges funding to projects 5000-9220 (FQ-PAIP) and IA-201024 (DGAPA-PAPIIT). We thank M. Flores-Álamo for collecting the X-ray diffraction data.

REFERENCES

1 J. Song, H. Lee, E. G. Jeong, K. C. Choi and S. Yoo, *Advanced Materials*, 2020, **32**, 1907539.
2 R. Achal, M. Rashidi, J. Croshaw, T. R. Huff and R. A. Wolkow, *ACS Nano*, 2020, **14**, 2947–2955.
3 L. Ceze, J. Nivala and K. Strauss, *Nat Rev Genet*, 2019, **20**, 456–466.
4 M. Vasilopoulou, A. Fakharuddin, A. G. Coutsolelos, P. Falaras, P. Argitis, Abd. R. bin M. Yusoff and M. K. Nazeeruddin, *Chem Soc Rev*, 2020, **49**, 4496–4526.
5 Y. Zhao, W. Liu, J. Zhao, Y. Wang, J. Zheng, J. Liu, W. Hong and Z.-Q. Tian, *International Journal of Extreme Manufacturing*, 2022, **4**, 022003.
6 A. R. Oganov, C. J. Pickard, Q. Zhu and R. J. Needs, *Nat Rev Mater*, 2019, **4**, 331–348.
7 J. G. P. Wicker and R. I. Cooper, *CrystEngComm*, 2015, **17**, 1927–1934.
8 T. R. Walsh, *Acc Chem Res*, 2017, **50**, 1617–1624.
9 G. R. Desiraju, *Angewandte Chemie International Edition in English*, 1995, **34**, 2311–2327.
10 J. Chen, C. L. Brooks and H. A. Scheraga, *J Phys Chem B*, 2008, **112**, 242–249.
11 H. M. Berman, W. K. Olson, D. L. Beveridge, J. Westbrook, A. Gelbin, T. Demeny, S. H. Hsieh, A. R. Srinivasan and B. Schneider, *Biophys J*, 1992, **63**, 751–759.
12 N. B. Leontis, *Nucleic Acids Res*, 2002, **30**, 3497–3531.
13 L. J. Prins, D. N. Reinhoudt and P. Timmerman, *Angewandte Chemie International Edition*, 2001, **40**, 2382–2426.
14 L. C. Gilday, S. W. Robinson, T. A. Barendt, M. J. Langton, B. R. Mullaney and P. D. Beer, *Chem Rev*, 2015, **115**, 7118–7195.
15 J. Ma, N. Han, H. Yu, J. Li, J. Shi, S. Wang, H. Zhang and M. Wang, *Small*, 2022, **18**, 202202167.
16 J.-H. Deng, J. Luo, Y.-L. Mao, S. Lai, Y.-N. Gong, D.-C. Zhong and T.-B. Lu, *Sci Adv*, 2020, **6**, eaax9976.
17 R. Arcos-Ramos, M. Maldonado-Domínguez, J. Ordóñez-Hernández, M. Romero-Ávila, N. Farfán and M. del P. Carreón-Castro, *J Mol Struct*, 2017, **1130**, 914–921.

18 E. González-Rodríguez, B. Guzmán-Juárez, M. Miranda-Olvera, M. del P. Carreón-Castro, M. Maldonado-Domínguez, R. Arcos-Ramos, N. Farfán and R. Santillan, *Spectrochim Acta A Mol Biomol Spectrosc*, 2022, **267**, 120520.
19 M. Maldonado-Domínguez, R. Arcos-Ramos, M. Romero, B. Flores-Pérez, N. Farfán, R. Santillan, P. G. Lacroix and I. Malfant, *New J. Chem.*, 2014, **38**, 260–268.
20 A. Vaitkus, A. Merkys, T. Sander, M. Quirós, P. A. Thiessen, E. E. Bolton and S. Gražulis, *J Cheminform*, 2023, **15**, 123.
21 A. Merkys, A. Vaitkus, A. Grybauskas, A. Konovalovas, M. Quirós and S. Gražulis, *J Cheminform*, 2023, **15**, 25.
22 A. Vaitkus, A. Merkys and S. Gražulis, *J Appl Crystallogr*, 2021, **54**, 661–672.
23 S. Gražulis, D. Chateigner, R. T. Downs, A. F. T. Yokochi, M. Quirós, L. Lutterotti, E. Manakova, J. Butkus, P. Moeck and A. Le Bail, *J Appl Crystallogr*, 2009, **42**, 726–729.
24 J.-S. Wu, W.-M. Liu, X.-Q. Zhuang, F. Wang, P.-F. Wang, S.-L. Tao, X.-H. Zhang, S.-K. Wu and S.-T. Lee, *Org Lett*, 2007, **9**, 33–36.
25 J. Ordóñez-Hernández, A. Jiménez-Sánchez, H. García-Ortega, N. Sánchez-Puig, M. Flores-Álamo, R. Santillan and N. Farfán, *Dyes and Pigments*, 2018, **157**, 305–313.
26 Agilent CrysAlis PRO and CrysAlis RED. Agilent Technologies, Yarnton, England, 2013.
27 R. C. Clark and J. S. Reid, *Acta Crystallogr A*, 1995, **51**, 887–897.
28 O. V. Dolomanov, L. J. Bourhis, R. J. Gildea, J. A. K. Howard and H. Puschmann, *J Appl Crystallogr*, 2009, **42**, 339–341.
29 C. F. Macrae, I. Sovago, S. J. Cottrell, P. T. A. Galek, P. McCabe, E. Pidcock, M. Platings, G. P. Shields, J. S. Stevens, M. Towler and P. A. Wood, *J Appl Crystallogr*, 2020, **53**, 226–235.
30 H. S. Yu, X. He, S. L. Li and D. G. Truhlar, *Chem Sci*, 2016, **7**, 5032–5051.
31 M. Cossi, N. Rega, G. Scalmani and V. Barone, *J Comput Chem*, 2003, **24**, 669–681.
32 H. Cui, K. Takahashi, Y. Okano, H. Kobayashi, Z. Wang and A. Kobayashi, *Angewandte Chemie International Edition*, 2005, **44**, 6508–6512.
33 J. Harada, M. Ohtani, Y. Takahashi and T. Inabe, *J Am Chem Soc*, 2015, **137**, 4477–4486.
34 V. Barone and M. Cossi, *J Phys Chem A*, 1998, **102**, 1995–2001.
35 R. Bauernschmitt and R. Ahlrichs, *Chem Phys Lett*, 1996, **256**, 454–464.
36 M. E. Casida, C. Jamorski, K. C. Casida and D. R. Salahub, *J Chem Phys*, 1998, **108**, 4439–4449.
37 R. E. Stratmann, G. E. Scuseria and M. J. Frisch, *J Chem Phys*, 1998, **109**, 8218–8224.
38 R. A. K. Yadav, D. K. Dubey, S.-Z. Chen, T.-W. Liang and J.-H. Jou, *Sci Rep*, 2020, **10**, 9915.
39 J. F. Janak, *Phys Rev B*, 1978, **18**, 7165–7168.
40 P. Politzer and F. Abu-Awwad, *Theoretical Chemistry Accounts: Theory, Computation, and Modeling (Theoretica Chimica Acta)*, 1998, **99**, 83–87.
41 S. Hamel, P. Duffy, M. E. Casida and D. R. Salahub, *J Electron Spectros Relat Phenomena*, 2002, **123**, 345–363.
42 D. Cagardová and V. Lukeš, *Acta Chimica Slovaca*, 2017, **10**, 6–16.